



Published in final edited form as:

ACS Biomater Sci Eng. 2020 November 09; 6(11): 6108–6116. doi:10.1021/acsbomaterials.0c01162.

Antibody Conjugate Assembly on Ultrasound-Confined Microcarrier Particles

Michael M. Binkley, Mingyang Cui, Mikhail Y. Berezin, J. Mark Meacham

Washington University in St. Louis, St. Louis, Missouri 63130, United States;

Abstract

Bioconjugates are important next-generation drugs and imaging agents. Assembly of these increasingly complex constructs requires precise control over processing conditions, which is a challenge for conventional manual synthesis. This inadequacy has motivated the pursuit of new approaches for efficient, controlled modification of high-molecular-weight biologics such as proteins, carbohydrates, and nucleic acids. We report a novel, hands-free, semiautomated platform for synthetic manipulation of biomolecules using acoustically responsive microparticles as three-dimensional reaction substrates. The microfluidic reactor incorporates a longitudinal acoustic trap that controls the chemical reactions within a localized acoustic field. Forces generated by this field immobilize the microscale substrates against the continuous flow of participating chemical reagents. Thus, the motion of substrates and reactants is decoupled, enabling exquisite control over multistep reaction conditions and providing high-yield, high-purity products with minimal user input. We demonstrate these capabilities by conjugating clinically relevant antibodies with a small molecule. The on-bead synthesis comprises capture of the antibody, coupling of a fluorescent tag, product purification, and product release. Successful capture and modification of a fluorescently labeled antibody are confirmed via fold increases of 49 and 11 in the green (antibody)- and red (small-molecule dye)-channel median intensities determined using flow cytometry. Antibody conjugates assembled on acoustically responsive, ultrasound-confined microparticles exhibit similar quality and quantity to those prepared manually by a skilled technician.

Graphical Abstract

Corresponding Author: J. Mark Meacham – Washington University in St. Louis, St. Louis, Missouri 63130, United States; Phone: 314-935-3821; meachamjm@wustl.edu.

Author Contributions

The manuscript was written through contributions of all authors. All authors have given approval to the final version of the manuscript.

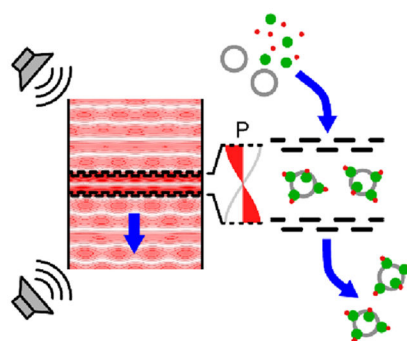
Complete contact information is available at: <https://pubs.acs.org/10.1021/acsbomaterials.0c01162>

Supporting Information

The Supporting Information is available free of charge at <https://pubs.acs.org/doi/10.1021/acsbomaterials.0c01162>.

Theoretical description of the mechanism responsible for acoustic confinement of microparticle reaction substrates; overview of the experimental setup for in-channel synthesis; details regarding hollow glass sphere functionalization and verification; assessment of antibody degradation following ultrasound exposure; and additional details regarding data collection and analysis ([PDF](#))

The authors declare no competing financial interest.



Keywords

acoustofluidics; microfluidics; antibody conjugates; solid-state chemistry; synthesis; automatic synthesis

INTRODUCTION

As the largest class of recognition molecules, antibodies are an integral tool for imaging,^{1,2} diagnosis,³ and therapy.^{4,5} Antibody conjugates (ACs) combine the high specificity of antibodies with biologically active drugs (antibody–drug conjugates, ADCs) or contrast agents (antibody–tracer conjugates, ATCs).^{6,7} Commonly used synthetic processes for biomolecules (including antibodies and proteins) rely on the classic *N*-hydroxysuccinimide (NHS) and maleimide-based conjugation,^{8,9} although other approaches have recently been developed for site-specific conjugations to antibodies.¹⁰ Intensive purification schemes to isolate the product from starting materials currently incorporate affinity chromatography (antibody conjugates) and diafiltration (protein conjugates) to minimize the presence of aggregates and to remove inherently-toxic free drug as appropriate.¹¹ This traditional manual synthesis of ACs is labor-intensive, requires large reagent volumes, and suffers from inconsistency and poor reproducibility.^{12,13} Thus, researchers seek alternative approaches to improve the synthetic methodology and enable scalable production of new ADCs and ATCs with less variability. Miniaturization and process automation offer possible solutions.¹³ Microfluidics enable noncontact, continuous-flow, and small-volume mixing, reaction, and/or separation of microparticles and nanomaterials (e.g., proteins and nucleic acids) in solution.^{14–18} Among these methods, acoustic microfluidics uses ultrasound to manipulate fluids,¹⁹ cells and cell-sized objects,^{20–22} and submicron particles.^{23,24} Acoustophoresis (or migration with sound) is label-free, relying only on differences in the inherent physical properties of the medium and suspended particles; however, it is also possible to tune the acoustophysical properties of species that are otherwise insensitive to the acoustic field. Affinity beads may be used for acoustophoretic segregation to achieve comparable purity and improved efficiency versus magnetic bead-based methods.²⁵

When suspended in an ultrasonic standing wave field, particles that are comparatively more rigid and denser than the fluid medium are driven to acoustic pressure minima (nodes).²⁶ The acoustic radiation force (termed F_{ARF} , see Figure 1) on a particle is a complex function of the field parameters (amplitude and frequency), particle size, and the degree of density

and compressibility mismatch between the particle and fluid, providing a means of differential fractionation and/or aggregation of select components from a heterogeneous mixture.^{27–29} Ultrasound in the low-MHz frequency range has little influence on the motion of submicron particles; however, acoustophoretic separation of nanomaterials has been achieved using higher frequency (>10 MHz) actuation of surface acoustic waves (SAW),²³ or attachment to biofunctionalized polymeric beads.^{30–32} Nanoscale proteins bound to the surface of microscale (1–10s of μm) carrier particles can be indirectly manipulated using low-MHz frequency bulk acoustic waves (BAW) where F_{ARF} on the particles overcomes flow drag (F_{d} in Figure 1).³³ Bead-mediated protein extraction via lateral separation under continuous flow (i.e., due to differing migration rates to low-pressure nodes oriented parallel to the direction of flow) has been reported,³⁴ but longitudinal enrichment perpendicular to the flow direction has not been demonstrated.

Herein, we adopt a unique acoustofluidic enrichment structure to allow for antibody (Ab) immobilization and modification on the surface of micron-sized carrier particles held in a longitudinal standing bulk acoustic wave (LSBAW).^{35,36} Nanoscale antibodies and other reagents are unaffected by acoustic radiation forces in the low-MHz range and thus, must be coupled to a microscale substrate for manipulation in the acoustic field.²³ Beyond Ab retention, we demonstrate conjugation, purification, and release of a modified protein using the synthetic process flow of Figure 1a. Briefly, hollow glass spheres (HGSs) coated by Protein G-terminated self-assembled monolayers (SAMs) are locally concentrated (focused) from a heterogeneous solution to the acoustic pressure node of the LSBAW microreactor. Here, they remain stationary during reagent flow and subsequent processing steps. Ab is captured, modified, and purified while bound to these SAMs (termed Ab-HGS complexes). A release buffer (low-pH solution) is used to detach the Ab from the Ab-HGS to allow for collection of products from the microchannel. Importantly, the device configuration facilitates removal and/or recycling of the excess Ab during AC incubation/purification.

An enrichment/trapping structure comprising pairs of perforated pseudowalls (i.e., porous walls that reflect acoustic waves but also permit undisrupted flow of the sample) is critical to LSBAW device operation (see schematic in Figure 1b). These features locally amplify the standing acoustic pressure field to balance drag forces during fluid flow.^{35,36} Thus, microcarrier particles are preferentially confined to a single prescribed location. The orthogonal orientation of the zero pressure node within the LSBAW trap contrasts that of prevailing acoustophoretic devices where nodes/antinodes are parallel to the inflow direction.^{37–39} Critical operating frequencies, which correspond to longitudinal half-wavelength resonances of the pillar array, exhibit a relative increase in acoustic energy density within the trap versus that of the channel inlet and outlet regions.^{35,36} The selected optimum operating frequency is intrinsic to the geometry of the microreactor, yielding predictable and consistent synthesis conditions. We used computer modeling to predict the harmonic response of the LSBAW channel, enabling identification of the desired first half-wavelength resonance for effective particle trapping and synthesis.

Precise control of complex synthetic processes is required to achieve the desired biological activity and specificity of a product; however, such precision is difficult to achieve using conventional, manual synthetic methods. The described LSBAW-based antibody conjugation

constitutes a multistep synthetic process (e.g., modification, purification, and release), with semiautomated control over reagent exchanges and incubation periods. Although AC production is used for proof-of-principle, results can be extended to other types of conjugations that benefit from controlled, serial exposure of stationary reaction substrates to different reagents.

RESULTS

Computational Modeling Guides Design of Acoustofluidic Device Architectures and Predicts Operating Conditions.

We have previously applied finite element analysis (FEA) and computational fluid dynamics (CFD) models to assess the trapping capability of various LSBAW geometries (Figure 2b,c).^{35,36} Eigenanalysis identified mode shapes (acoustic pressure fields) that were suitable for microparticle confinement perpendicular to the inflow direction. For the geometry shown in Figure 2, the optimal first half-wavelength resonance of the pillar structure was predicted to lie at a frequency of $f_{1,M} = 624$ kHz, but several similar eigenshapes were found between 540 and 630 kHz.^{35,36} At these frequencies, the pillar arrays that comprise the microreactor act as pseudowalls to augment the local field, forming a pressure well along the midline of the acoustic trap (Figure 2b). The nodal plane confines reaction substrates to a single band for facile monitoring of the in-channel synthesis. To validate the computational model, the transducer was swept over possible actuation frequencies of a channel seeded with 10 μm diameter polystyrene (PS) microparticles (1×10^6 beads per 1 mL of deionized water). The experimental operating frequency was found at $f_{1,E} = 575$ kHz [which was consistent for experiments using PS beads and HGS reaction substrates, see Figure 3b(i,ii)]. Here, beads arranged in a linear band perpendicular to the inflow direction demonstrating that the glass LSBAW chip shown in Figure 2e provides a robust trapping condition. A drive voltage of 91 V_{pp} was sufficient to retain particles against an inflow rate of 7 $\mu\text{L}/\text{min}$ [Figure 3b(ii-iv)], which was the reagent flowrate used throughout the synthesis. CFD results (Figure 2c, flow rate $Q_M = 100$ $\mu\text{L}/\text{min}$) indicate that laminar flow behavior is expected even at flow rates that far exceed the current experimental operating conditions.

Longitudinal Acoustic Trapping Enables Localized Antibody Binding and Purification on Static Three-Dimensional Substrates.

Having identified the optimal experimental operating condition, we demonstrate that the LSBAW-based microreactor can efficiently perform the first step of the antibody conjugate (AC) synthesis, namely, capturing the Ab on the surface of particles with a positive acoustic contrast factor ($\Phi > 0$, i.e., particle is denser and less compressible than the fluid medium). Prepared Protein G-terminated HGSs (see the Supporting Information and Figure S2a–d) were introduced into the microreactor channel prior to LSBAW actuation to form a uniform bead distribution within the pillar array [Figure 3b(i)]. Upon actuation at the first half-wavelength resonance of the pillar structure ($f_{1,E} = 575$ kHz, $V_E = 91$ V_{pp}), HGS agglomerated in a well-defined, linear band at the microreactor midline between the two opposing pillar arrays [Figure 3b(ii)]. Phosphate-buffered saline (PBS) solution was then used to wash the beads and remove free (unfocused) HGS and other particles smaller than the critical size needed for the acoustic radiation force to overcome viscous drag.

A fluorescently labeled Ab (Alexa Fluor 488, AF488) solution was introduced and incubated with the beads for 45 min. Fluorescence imaging confirmed the successful capture of the Ab by the beads through strong binding of Protein G to the Ab [Figure 3b(iii)]. After a subsequent PBS wash, Ab-decorated HGS (Ab-HGS) remained trapped at the microreactor midline, and excess reagents had been removed from the channel [Figure 3b(iv)]. Ab to HGS binding was continually monitored during the synthesis by measuring the intensity of the bead agglomerate (I_{bead}), the pillar array (I_{pillar}), and their difference ($I = I_{\text{bead}} - I_{\text{pillar}}$). As shown in Figure 3c, I reached a maximum at 15 min of incubation with the Ab solution and remained high after the removal of excess free Ab. Note that total incubation times for all processes were selected to approximate the timing of the manual steps. Here, we observed that the beads reached a maximum intensity well before the total incubation time of 45 min. This result confirmed that antibodies were bound to the surface of the HGS. Furthermore, negligible I_{pillar} post-PBS wash indicated complete reagent replacement within the microchannel during the specified wash time. The Ab was removed from the beads using a low-pH release buffer of 2% HCl (aq.). In that case, almost complete recovery of the Ab can be achieved as supported by the postrelease reduction in fluorescence shown in Figure 3c. The antibodies also appeared to be stable in the acoustic standing wave at the experimental operating frequency. No changes in the molecular weight of the Ab after exposure to the LSBAW conditions were observed (see the Supporting Information and Figure S3). This stability is critical for any pharmacological application where the integrity of the drug ensures its safety profile.

LSBAW-Based Antibody–Dye Conjugation Realizes a Complete Synthetic Process.

After verifying that the core processing steps of Ab capture, wash, and release can be completed under LSBAW operating conditions, we next establish the feasibility of applying the method to biomolecule modification. To illustrate synthetic applicability, we conjugated an Ab with a fluorescent tag. *N*-hydroxysuccinimide (NHS) chemistry—a common method that targets free amine groups for preparation of antibody-drug conjugates (ADCs)⁴⁰—was used to react the bound Ab with a preactivated NHS ester of the red fluorescent dye sulfo-Cyanine3 (Cy3) in a LSBAW microreactor. Again, the excess free dye was removed using a PBS wash. Conjugated products were cleaved from the surface of the beads using the release buffer and collected at the outlet. Antibody–tracer conjugates (ATCs) were synthesized on-chip and using a manual process for comparison of reaction products. The synthetic steps for these protocols are given in Figure 4, along with the nomenclature used to represent intermediate products (samples **I–VI**; on-chip **a**; manual **b**) for both reaction pathways (see also the Experimental Procedures section).

The multistep LSBAW-based conjugation process was assessed using fluorescence microscopy *in situ* (continuously monitored) and flow cytometry *ex situ* (at discrete points throughout the synthesis progression). A complete comparison of the flow cytometry intensity scatter plots for manual, on bead-prepared controls and LSBAW microreactor-synthesized products is provided in Figure S5, for reference. Scatter plots for the green (FITC) and red (Cy3) channels prior to modification, after Cy3 addition, and after Ab release are shown in Figure 5. The brightfield, green, and red composite image shown in the inset of Figure 5a demonstrates collection of Protein G-terminated HGSs (sample **II**) under

the acoustic actuation. Aggregation evidences the effect of the ultrasonic standing wave on the beads, enabling HGS localization and concentration to a specific region within the reaction chamber. A lack of fluorescence for sample **II** was confirmed by both fluorescence imaging (Figure 5a and Figure S4e,f) and flow cytometry (Figure 5a). LSBAW-based capture of the AF488 Ab to the bead surface followed by conjugation of the red Cy3-NHS ester to the same Ab led to an increase of the fluorescence in both the green and red channels for sample **IVa** (Figure 5b). A quantitative comparison of samples **II** and **IVa** indicated that fluorescence of the clusters containing double-labeled antibodies was greatly increased in both green [Kolmogorov–Smirnov (K-S) algorithm, $p < 0.001$, see the Experimental Procedures section] and red (K-S, $p < 0.001$) channels. The composite image of the brightfield, green, and red fluorescence micrographs (inset Figure 5b) shows the overlap in color, appearing as orange/yellow, to be uniform exclusively across the bead cluster. While certain amino acids comprising Protein G are known to autofluoresce,^{41,42} the intensities of the modified Ab-decorated HGS (Ab-HGS) sample **IVa** were 2–3 orders of magnitude larger than those of the unmodified sample **II**. Brightfield, green-channel, and red-channel images of the unmodified control sample **II** and on-chip processed sample **IVa** support this conclusion (Figure S4). In addition, the larger increase in intensity of the red channel for sample **IVa** versus a Protein G-terminated HGS control that was incubated with Cy3 indicates that alteration of the Ab occurred alongside lysine modification of Protein G (Figure S5).⁴² Thus, the Ab was bound and Cy3 dye was successfully coupled to the immobilized Ab.

Acidic treatment of the acoustically confined beads effects separation of the double-labeled antibodies (sample **VIa**) from the beads (sample **Va**), which were collected at the outlet under no acoustic actuation. Flow cytometry (Figure 5c) of the decoupled beads indicates the possibility of high collection efficiency for the modified Ab. Intensity in both the red and green channels was significantly reduced ($p < 0.0001$) after treatment with the release buffer demonstrating surface detachment (Figure 5c); however, neither the green- nor red-channel intensities of sample **Va** returned to the initial values of sample **II**, possibly due to incomplete decoupling or shielding of the HGS surface, which prevented buffer penetration into the bead cluster. Due to the significant reduction in signal for both channels, we also conclude that the low-pH buffer cleaved at the location of the Protein G and did not preferentially react with the Cy3 conjugation.

On-Chip Antibody Conjugation Reproduces Manual On-Bead Synthesis.

Finally, we show that the LSBAW-based conjugation of Cy3 to AF488 antibodies bound to HGS (Ab-HGS) is comparable to manually prepared Cy3-modified Ab-HGS constructs. Intensity scatter plots and histograms for LSBAW-based and manually synthesized Cy3-modified Ab-HGS exhibited similar green (FITC)- and red (Cy3)-channel distributions (Figure 6). The median and interquartile range (IQR) of the green-channel intensity were 636.9 (296.8, 1370.7) a.u. and 842.8 (379.1, 1790.3) a.u. for the LSBAW- and manually synthesized samples, respectively. Median and IQR of the red-channel intensity were 165.8 (90.7, 228.8) a.u. for the LSBAW-based sample and 233.0 (116.0, 515.8) a.u. for the manually synthesized sample. Thus, based on the overall population scatter and intensity

histograms, the median intensity and intensity variability for beads modified on-chip were found to approximate those of the manually synthesized control.

DISCUSSION

Capture microparticles modify the acoustophysical properties of nanoscale biomolecules to significantly increase their susceptibility to low-MHz ultrasonic actuation.^{30–32,34} Previous studies anticipate a number of potential applications involving acoustofluidic manipulation of nanomaterials; however, results are limited to single unit operations (e.g., concentration, separation, or fractionation of heterogeneous mixtures). For example, acoustic radiation forces have been used to agglomerate reaction substrates without flow⁴³ and to remove reaction byproducts through translation of micro-carriers into nonreacting buffer solutions.^{34,44} In conventional acoustophoresis, acoustic pressure nodes are oriented parallel to the flow direction, and lateral movement/separation occurs as particles proceed along a microchannel. Because particle motion is coupled to the fluid motion by flow drag, it is difficult to perform more than a single reagent exchange/wash before diffusion leads to the homogenization of coflowing sample streams.

In the present work, we incorporate a longitudinal acoustic trap that creates a pressure well perpendicular to the microreactor sample inflow. Coincident application of primary acoustic radiation forces and flow drag decouples particle and fluid motion. Reaction substrates are confined to a predefined location as processing conditions (e.g., reagent/buffer composition and residence time) are varied. Thus, the LSBAW configuration enables a sequence of operations constituting a complete synthetic process: (i) biomolecule capture, (ii) modification, (iii) purification, and (iv) release.

Computational modeling is applied to identify candidate microreactor resonant frequencies where the LSBAW structure augments the local pressure field to form a single acoustic pressure minimum for substrate confinement.^{35,36} To this end, the eigenanalysis provides a useful qualitative description of the device harmonic response (Figures 2b and 3a). FEA and CFD models can be integrated to allow for future optimization of the LSBAW architecture regarding flow and/or acoustic confinement.⁴⁵ The current microreactor geometry (pillar size, shape, and configuration) was originally designed for rare species enrichment where high volumetric throughput is critical; however, high throughput is less important than a high trapping capacity for synthesis applications. We expect improved performance from the next generation of LSBAW microreactors that comprise multiple arrays of closely spaced pillars with larger acoustic cross sections. Furthermore, the design of the microreactor is well-suited to conventional microfluidic scale-up strategies to increase capacity (e.g., creating a series of sequential trapping zones in the flow direction and/or arraying multiple LSBAW microchannels to operate in parallel). Regardless, the nonoptimized device reported here establishes the compelling features of the LSBAW platform for controlled biomolecule synthesis.

Microparticle reaction substrates are consistently trapped and held against the bulk flow of reagents at the selected LSBAW operating frequency. We have observed vortical flows around the bead agglomerates in LSBAW devices, which can enhance reagent transport

compared to microfluidic packed-bed reactors and wall-based reactors with limited surface area to volume ratios.^{36,46,47} Local mixing also promotes uniform exposure of the three-dimensional substrate surfaces to fresh reagents. We expect that these attributes (predictable operation and enhanced transport characteristics) can address extant issues with AC synthesis, leading to custom AC production with less variability. In the reported work, on-chip LSBAW-based Ab immobilization and modification produced an AC that was virtually the same as that synthesized manually. The biocompatibility of exposure to ultrasound in acoustic microfluidics has been evaluated at the cellular and molecular levels.^{48–50} Our results confirm that acoustic actuation does not affect Ab molecular weight, though additional analyses to assess binding capability before and after treatment are needed. Although we used the well-established NHS conjugation, the method can be easily expanded to many other types of conjugation, including site-specific.^{51,52} Beyond biomolecule synthesis, our proof-of-principle establishes a framework for future studies that utilize ultrasound-confined microcarrier particles for detection and continuous process monitoring. For example, antibody decorated substrates can bind and detect the free antigen in solution. Thus, the LSBAW platform is well-suited to a range of applications, from ex vivo cancer assays and diagnostics (e.g., enzyme-linked immunosorbent assay, ELISA) to imaging (antibody-tracer conjugates) and interventions (antibody-drug conjugates).

EXPERIMENTAL PROCEDURES

Substrate Confinement Mechanism.

For the heterogeneous particle systems included in the present study, only the HGS substrates experience a non-negligible acoustic radiation force F_{ARF} due to the size dependence of the force amplitude ($|F_{\text{ARF}}| \sim a^3$ where a is the particle radius). F_{ARF} is also dependent on the acoustophysical properties of the particles and medium, and the amplitude and frequency of the acoustic field (see complete description in the Supporting Information). The LSBAW microreactor was designed such that F_{ARF} exceeded the flow drag F_{d} on HGS at typical reagent inflow rates to halt the motion of the microscale substrates relative to the nanoscale reagents in solution.

Computational Modeling.

A two-dimensional (2D) finite element analysis (FEA) and laminar flow computational fluid dynamics (CFD) model were created in the commercial software COMSOL Multiphysics with the acoustics and microfluidics modules.⁵³ Computational models were used to predict the LSBAW-channel harmonic response and flow field. The eigenanalysis considered only the fluid domain (water; density $\rho_w = 998 \text{ kg/m}^3$ and speed of sound $c_w = 1481 \text{ m/s}$), and sound hard boundary conditions were applied to all solid–liquid interfaces. Eigenfrequencies and eigenmodes (pressure fields) suitable for HGS confinement were identified by maxima of the ratio of acoustic energy density in the LSBAW trap to that in the inlet/outlet regions.³⁵ For the laminar flow model, the predicted velocity at the midline of the trap remained below 1.0 cm/s, even for a nominal inflow rate of 100 $\mu\text{L}/\text{min}$, which is an order of magnitude larger than the experimental rate of 7 $\mu\text{L}/\text{min}$.

Channel Fabrication.

The LSBAW microchannel was fabricated using standard isotropic wet etching [2:1:6 (vol.), hydrofluoric acid (aq., 49%):nitric acid (aq., 69%):deionized water] of a photolithographically patterned 63.5 mm × 63.5 mm × 1.5 mm thick chrome-coated soda-lime glass mask blank (Telic Co.) to a depth of ~60 μm . The glass microchannel was enclosed by a second blank using a calcium-assisted bonding technique.⁵⁴ The channel volume was approximately 41 μL .

LSBAW Device Assembly and Operation.

A 24 mm × 28 mm × 1.5 mm thick PZT-8 piezoelectric transducer (APC 880, American Piezo Ceramics, Inc.) was clamped to the glass LSBAW microchannel using ultrasound gel (McKesson Corp.) as an acoustic coupling medium. The assembly was placed on the stage of an inverted microscope (Axio Observer z.1, Carl Zeiss AG) to monitor synthesis progression (see the Supporting Information and Figure S1). Inlet/outlet tubing was held in place using microfluidic probes (CorSolutions, LLC). The transducer was driven using an amplified ac signal (33522A, Agilent Technologies, Inc.; 2100L, Electronic Navigation Industries). The optimal first half-wavelength resonance ($f_{1,E} = 575$ kHz, $V_E = 91$ V_{pp}) was identified by scanning over a 90-kHz range covering the (nominal) model-predicted frequency range from 540–630 kHz. Reagents were introduced at a controlled flow rate of 7 $\mu\text{L}/\text{min}$ using a syringe pump (Legato 110, KD Scientific, Inc.). Reagent changes occurred over 15 min (~2.5 times the total microchannel volume) to ensure complete reagent removal and replacement of the microreactor volume.

Hollow Glass Sphere Functionalization.

The surface of borosilicate HGSs (6 $\mu\text{m} \pm 3.5$ μm diameter; HGS-10, Dantec Dynamics A/S) was modified to create a self-assembled monolayer (SAM) with terminal Protein G for Ab binding. A detailed description of surface chemistry development and verification is provided in the Supporting Information and Figure S2.

Antibody Modification in the LSBAW Microreactor.

The acoustically confined HGSs with surface-bound antibodies were treated for 2 h in a solution of sulfo-Cyanine3 (Cy3)-NHS ester (Lumiprobe Corp.) dissolved in a pH 8.0 buffer (potassium phosphate monobasic/sodium hydroxide, Fisher Scientific Co.) to 2 mg dye per 1 mL buffer. The reagent solution was introduced at 7 $\mu\text{L}/\text{min}$ for 15 min and incubated at 23 °C for 2 h before removal using a 1 × PBS wash (7 $\mu\text{L}/\text{min}$ for 15 min). Acoustic actuation was exclusively used during reagent introduction and the buffer wash as a precaution to minimize heating and/or potential damage due to ultrasound exposure during incubation.

Assessment of Antibody Degradation Following Ultrasound Exposure.

Gel electrophoresis was used to compare the molecular weight of an untreated control, a flow-only control, and antibodies exposed to flow conditions and ultrasound equivalent to that used for the synthesis. The detailed procedure and gel electrophoresis results are provided in the Supporting Information and Figure S3. Results indicate no change in

molecular weight after treatment at the experimental flowrate and acoustic pressure. Bands for all samples indicated >130 kDa molecular weight.

Fluorescence Microscopy and Flow Cytometry.

Binding of a fluorescent Ab (rabbit anti-goat IgG AF488, Abcam, Inc.) and coupling of the Cy3-NHS ester (Lumiprobe Corp.) were assessed using fluorescence microscopy (Axio Observer z.1, Carl Zeiss AG) and flow cytometry (LSR Fortessa, BD Biosciences). Brightfield, green-channel (FITC, $\lambda_{\text{ex}} = 470/40$ nm, $\lambda_{\text{em}} = 525/50$ nm), and red-channel (Cy3, $\lambda_{\text{ex}} = 546/12$ nm, $\lambda_{\text{em}} = 575\text{--}640$ nm) images were captured as single-channel and composite images to monitor the progression of synthesis. Exposure times varied depending on the magnification level but were consistent across each experiment, as described earlier. Flow cytometry calibration and data collection are described in the Supporting Information. Due to inherent HGS heterogeneity, no gating was applied (i.e., the population distributions included all events). Any shifts in fluorescence were attributed to antibody coupling/decoupling and modification. Selection of fluorophores with distinct emission spectra obviated the need for compensation.

Statistical Methods.

Intensity values obtained from flow cytometry are presented as the median and the interquartile range (25th and 75th percentile, respectively). Statistical comparison of the resulting histograms was conducted in FloJo v.10⁵⁵ using the Kolmogorov–Smirnov (K-S) algorithm. Significant p-values indicate that the samples come from different population distributions.

Supplementary Material

Refer to Web version on PubMed Central for supplementary material.

ACKNOWLEDGMENTS

The reported work was supported by the National Cancer Institute and the National Heart, Lung, and Blood Institute of the National Institutes of Health under Award Nos. 1R01CA208623 and 5T32HL007317, and by a Washington University School of Engineering and Applied Sciences Collaboration Initiation Grant. The authors thank the technical staffs at the Institute of Materials Science and Engineering at Washington University in St. Louis and the Flow Cytometry and Fluorescence Activated Cell Sorting Core at Washington University School of Medicine in St. Louis who provided resources and assistance in fabrication and data collection and analysis.

Funding

National Cancer Institute, National Institutes of Health Award No. 1R01CA208623. National Heart, Lung, and Blood Institute, National Institutes of Health Award No. 5T32HL007317. Washington University School of Engineering and Applied Sciences Collaboration Initiation Grant.

ABBREVIATIONS

Ab	antibody
AC	antibody conjugate
ADC	antibody-drug conjugate

ATC	antibody-tracer conjugate
BAW	bulk acoustic wave
CFD	computational fluid dynamics
ELISA	enzyme-linked immunosorbent assay
F_{ARF}	acoustic radiation force
F_{d}	flow drag
FEA	finite element analysis
HGS	hollow glass sphere
Ab-HGS	antibody-hollow glass sphere
IQR	interquartile range
LSBAW	longitudinal standing bulk acoustic wave
NHS	<i>N</i> -hydroxysuccinimide
PBS	phosphate buffered saline
SAM	self-assembled monolayer
SAW	surface acoustic wave

REFERENCES

- (1). Scheinberg D; Strand M; Gansow O Tumor imaging with radioactive metal chelates conjugated to monoclonal antibodies. *Science* 1982, 215, 1511–1513. [PubMed: 7199757]
- (2). Sano K; Mitsunaga M; Nakajima T; Choyke PL; Kobayashi H In vivo breast cancer characterization imaging using two monoclonal antibodies activatably labeled with near infrared fluorophores. *Breast Cancer Res.* 2012, 14, R61. [PubMed: 22510481]
- (3). Borrebaeck CA Antibodies in diagnostics—from immunoassays to protein chips. *Immunol. Today* 2000, 21, 379–382. [PubMed: 10916140]
- (4). Willett CG; Boucher Y; Di Tomaso E; Duda DG; Munn LL; Tong RT; Chung DC; Sahani DV; Kalva SP; Kozin SV Direct evidence that the VEGF-specific antibody bevacizumab has antivasculature effects in human rectal cancer. *Nat. Med* 2004, 10, 145–147. [PubMed: 14745444]
- (5). Chames P; Van Regenmortel M; Weiss E; Baty D Therapeutic antibodies: successes, limitations and hopes for the future. *Br. J. Pharmacol* 2009, 157, 220–233. [PubMed: 19459844]
- (6). Cazzamalli S; Dal Corso A; Widmayer F; Neri D Chemically defined antibody- and small molecule-drug conjugates for in vivo tumor targeting applications: A comparative analysis. *J. Am. Chem. Soc* 2018, 140, 1617–1621. [PubMed: 29342352]
- (7). Carter PJ; Lazar GA Next generation antibody drugs: pursuit of the ‘high-hanging fruit’. *Nat. Rev. Drug Discovery* 2018, 17, 197–223. [PubMed: 29192287]
- (8). Agarwal P; Bertozzi CR Site-specific antibody-drug conjugates: the nexus of bioorthogonal chemistry, protein engineering, and drug development. *Bioconjugate Chem.* 2015, 26, 176–192.
- (9). Behrens CR; Liu B Methods for site-specific drug conjugation to antibodies. *mAbs* 2014, 6, 46–53. [PubMed: 24135651]

- (10). Kishimoto S; Nakashimada Y; Yokota R; Hatanaka T; Adachi M; Ito Y Site-specific chemical conjugation of antibodies by using affinity peptide for the development of therapeutic antibody format. *Bioconjugate Chem.* 2019, 30, 698–702.
- (11). Wilson R A personal perspective of the development and validation of a phase-specific antibody-drug conjugate cytotoxicity potency assay. *Bioanalysis* 2013, 5, 1083–1097. [PubMed: 23641698]
- (12). Novosad JA; Kalantaridou SN; Tong Z-B; Nelson LM Ovarian antibodies as detected by indirect immunofluorescence are unreliable in the diagnosis of autoimmune premature ovarian failure: a controlled evaluation. *BMC Women's Health* 2003, 3, 2. [PubMed: 12694633]
- (13). Rameez S; Mostafa SS; Miller C; Shukla AA High-throughput miniaturized bioreactors for cell culture process development: Reproducibility, scalability, and control. *Biotechnol. Prog* 2014, 30, 718–727. [PubMed: 24449637]
- (14). Weigl BH; Yager P Microfluidic diffusion-based separation and detection. *Science* 1999, 283, 346–347.
- (15). Creamer JS; Oborny NJ; Lunte SM Recent advances in the analysis of therapeutic proteins by capillary and microchip electrophoresis. *Anal. Methods* 2014, 6, 5427–5449. [PubMed: 25126117]
- (16). Millet LJ; Lucheon JD; Standaert RF; Retterer ST; Doktycz MJ Modular microfluidics for point-of-care protein purifications. *Lab Chip* 2015, 15, 1799–1811. [PubMed: 25740172]
- (17). Li F; Guijt RM; Breadmore MC Nanoporous membranes for microfluidic concentration prior to electrophoretic separation of proteins in urine. *Anal. Chem* 2016, 88, 8257–8263. [PubMed: 27391148]
- (18). Kant K; Shahbazi M-A; Dave VP; Ngo TA; Chidambara VA; Than LQ; Bang DD; Wolff A Microfluidic devices for sample preparation and rapid detection of foodborne pathogens. *Biotechnol. Adv* 2018, 36, 1003–1024. [PubMed: 29534915]
- (19). Sriharan K; Strobl CJ; Schneider MF; Wixforth A; Guttenberg Z Acoustic mixing at low Reynold's numbers. *Appl. Phys. Lett* 2006, 88, No. 054102.
- (20). Ai Y; Sanders CK; Marrone BL Separation of *Escherichia coli* bacteria from peripheral blood mononuclear cells using standing surface acoustic waves. *Anal. Chem* 2013, 85, 9126–9134. [PubMed: 23968497]
- (21). Antfolk M; Magnusson C; Augustsson P; Lilja H; Laurell T Acoustofluidic, label-free separation and simultaneous concentration of rare tumor cells from white blood cells. *Anal. Chem* 2015, 87, 9322–9328. [PubMed: 26309066]
- (22). Xu T; Soto F; Gao W; Dong R; Garcia-Gradilla V; Magaña E; Zhang XJ; Wang J Reversible swarming and separation of self-propelled chemically powered nanomotors under acoustic fields. *J. Am. Chem. Soc* 2015, 137, 2163–2166. [PubMed: 25634724]
- (23). Destgeer G; Ha BH; Jung JH; Sung HJ Submicron separation of microspheres via travelling surface acoustic waves. *Lab Chip* 2014, 14, 4665–4672. [PubMed: 25312065]
- (24). Wu M; Chen C; Wang Z; Bachman H; Ouyang Y; Huang P-H; Sadovsky Y; Huang TJ Separating extracellular vesicles and lipoproteins via acoustofluidics. *Lab Chip* 2019, 19, 1174–1182. [PubMed: 30806400]
- (25). Urbansky A; Lenshof A; Dykes J; Laurell T; Scheduling S Affinity-bead-mediated enrichment of CD8+ lymphocytes from peripheral blood progenitor cell products using acoustophoresis. *Micromachines* 2016, 7, 101.
- (26). Bruus H Acoustofluidics 7: The acoustic radiation force on small particles. *Lab Chip* 2012, 12, 1014–1021. [PubMed: 22349937]
- (27). King LV On the Acoustic Radiation Pressure on Spheres. *Proc. R. Soc. A* 1934, 147, 212–240.
- (28). Yosioka K; Kawasima Y Acoustic radiation pressure on a compressible sphere. *Acta Acustica United Acustica* 1955, 5, 167–173.
- (29). Gor'Kov L On the forces acting on a small particle in an acoustical field in an ideal fluid. *Dokl. Akad. Nauk SSSR* 1961, 140, 88.
- (30). Shields CW IV; Sun D; Johnson KA; Duval KA; Rodriguez AV; Gao L; Dayton PA; López GP Nucleation and growth synthesis of siloxane gels to form functional, monodisperse, and acoustically programmable particles. *Angew. Chem., Int. Ed* 2014, 53, 8070–8073.

- (31). Tenje M; Xia H; Evander M; Hammarström B; Tojo A; Belák S; Laurell T; LeBlanc N Acoustic trapping as a generic noncontact incubation site for multiplex bead-based assays. *Anal. Chim. Acta* 2015, 853, 682–688. [PubMed: 25467518]
- (32). Ahmad R; Destgeer G; Afzal M; Park J; Ahmed H; Jung JH; Park K; Yoon T-S; Sung HJ Acoustic wave-driven functionalized particles for aptamer-based target biomolecule separation. *Anal. Chem* 2017, 89, 13313–13319. [PubMed: 29148722]
- (33). Lenshof A; Magnusson C; Laurell T Acoustofluidics 8: Applications of acoustophoresis in continuous flow microsystems. *Lab Chip* 2012, 12, 1210–1223. [PubMed: 22362021]
- (34). Augustsson P; Persson J; Ekström S; Ohlin M; Laurell T Decomplexing biofluids using microchip based acoustophoresis. *Lab Chip* 2009, 9, 810–818. [PubMed: 19255663]
- (35). Cui M; Binkley MM; Shekhani HN; Berezin MY; Meacham JM Augmented longitudinal acoustic trap for scalable microparticle enrichment. *Biomicrofluidics* 2018, 12, No. 034110. [PubMed: 29937950]
- (36). Binkley MM; Cui M; Li W; Tan S; Berezin MY; Meacham JM Design, modeling, and experimental validation of an acoustofluidic platform for nanoscale molecular synthesis and detection. *Phys. Fluids* 2019, 31, No. 082007.
- (37). Antfolk M; Antfolk C; Lilja H; Laurell T; Augustsson P A single inlet two-stage acoustophoresis chip enabling tumor cell enrichment from white blood cells. *Lab Chip* 2015, 15, 2102–2109. [PubMed: 25824937]
- (38). Antfolk M; Laurell T Continuous flow microfluidic separation and processing of rare cells and bioparticles found in blood—A review. *Anal. Chim. Acta* 2017, 965, 9. [PubMed: 28366216]
- (39). Zalis MC; Reyes JF; Augustsson P; Holmqvist S; Roybon L; Laurell T; Deierborg T Label-free concentration of viable neurons, hESCs and cancer cells by means of acoustophoresis. *Integr. Biol* 2016, 8, 332–340.
- (40). Sochaj AM; widerska KW; Otlewski J Current methods for the synthesis of homogeneous antibody–drug conjugates. *Biotechnol. Adv* 2015, 33, 775–784. [PubMed: 25981886]
- (41). Chen Y; Barkley MD Toward understanding tryptophan fluorescence in proteins. *Biochemistry* 1998, 37, 9976–9982. [PubMed: 9665702]
- (42). Sjöbring U; Björck L; Kastern W Streptococcal protein G. Gene structure and protein binding properties. *J. Biol. Chem* 1991, 266, 399–405. [PubMed: 1985908]
- (43). Ruedas-Rama MJ; Domínguez-Vidal A; Radel S; Lendl B Ultrasonic trapping of microparticles in suspension and reaction monitoring using Raman microspectroscopy. *Anal. Chem* 2007, 79, 7853–7857. [PubMed: 17874849]
- (44). Norris JV; Evander M; Horsman-Hall KM; Nilsson J; Laurell T; Landers JP Acoustic differential extraction for forensic analysis of sexual assault evidence. *Anal. Chem* 2009, 81, 6089–6095. [PubMed: 19591449]
- (45). Ledbetter AD; Shekhani HN; Binkley MM; Meacham JM Tuning the coupled-domain response for efficient ultrasonic droplet generation. *IEEE Trans. Ultrason. Ferroelectr. Freq. Control* 2018, 65, 1893–1904. [PubMed: 30047875]
- (46). Seong GH; Heo J; Crooks RM Measurement of enzyme kinetics using a continuous-flow microfluidic system. *Anal. Chem* 2003, 75, 3161–3167. [PubMed: 12964765]
- (47). Bai Y; Koh CG; Boreman M; Juang Y-J; Tang I-C; Lee LJ; Yang S-T Surface modification for enhancing antibody binding on polymer-based microfluidic device for enzyme-linked immunosorbent assay. *Langmuir* 2006, 22, 9458–9467. [PubMed: 17042569]
- (48). Burguillos MA; Magnusson C; Nordin M; Lenshof A; Augustsson P; Hansson MJ; Elmér E; Lilja H; Brundin P; Laurell T; Deierborg T Microchannel acoustophoresis does not impact survival or function of microglia, leukocytes or tumor cells. *PLoS One* 2013, 8, e64233. [PubMed: 23724038]
- (49). Wiklund M Acoustofluidics 12: Biocompatibility and cell viability in microfluidic acoustic resonators. *Lab Chip* 2012, 12, 2018–2028. [PubMed: 22562376]
- (50). Cushing KW; Piyasena ME; Carroll NJ; Maestas GC; López BA; Edwards BS; Graves SW; López GP Elastomeric negative acoustic contrast particles for affinity capture assays. *Anal. Chem* 2013, 85, 2208–2215. [PubMed: 23331264]

- (51). St Amant AH; Huang F; Lin J; Lemen D; Chakiath C; Mao S; Fazenbaker C; Zhong H; Harper J; Xu W; Patel N; Adams L; Vijaykrishnan B; Howard PW; Marelli M; Wu H; Gao CS; de Alaniz JR; Christie RJ A reactive antibody platform for one-step production of antibody-drug conjugates through a Diels-Alder reaction with maleimide. *Bioconjugate Chem.* 2019, 30, 2340–2348.
- (52). VanBrunt MP; Shanebeck K; Caldwell Z; Johnson J; Thompson P; Martin T; Dong HF; Li GR; Xu HY; D’Hooge F; Masterson L; Bariola P; Tiberghien A; Ezeadi E; Williams DG; Hartley JA; Howard PW; Grabstein KH; Bowen MK; Marelli M Genetically encoded azide containing amino acid in mammalian cells enables site-specific antibody-drug conjugates using click cycloaddition chemistry. *Bioconjugate Chem.* 2015, 26, 2249–2260.
- (53). COMSOL Multiphysics v. 5.2a 2016, COMSOL AB, Stockholm, Sweden.
- (54). Allen PB; Chiu DT Calcium-assisted glass-to-glass bonding for fabrication of glass microfluidic devices. *Anal. Chem* 2008, 80, 7153–7157. [PubMed: 18690699]
- (55). FlowJo Software (for Windows) v. 10. 2019, Becton, Dickinson, and Company, Ashland, Oregon, USA.

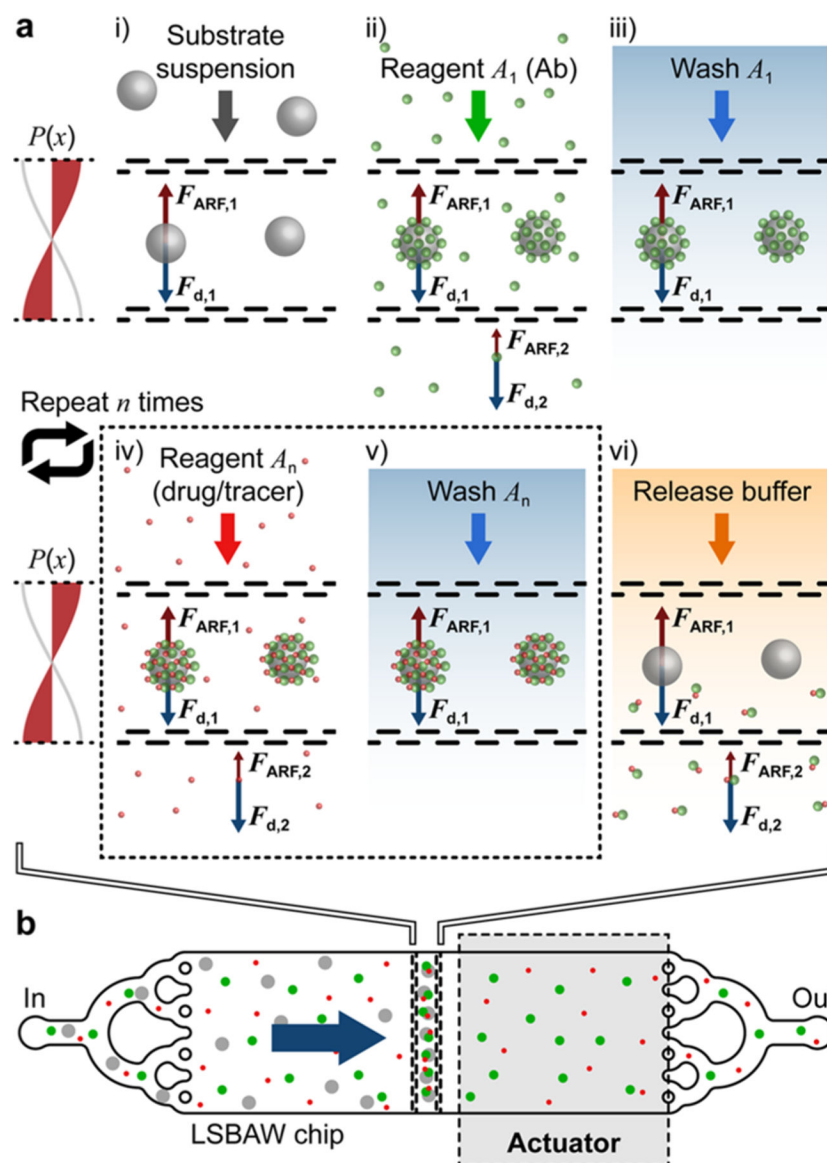


Figure 1. Concept overview for LSBAW-mediated synthesis on ultrasound-confined microparticle substrates. (a) Antibody (Ab) capture, modification, purification, and release protocol: (i) Protein G-coated microparticles are confined to the acoustic pressure node of an LSBAW microreactor; (ii) reagent A_1 (Ab solution) is introduced, and Ab is immobilized on the reaction substrates; (iii) remaining Ab is washed away with a buffer solution; (iv) and (v) bound Ab is modified and purified through a sequential introduction and washing of additional reagents A_n ; and (vi) a release buffer is used to detach modified Ab for collection at the outlet. (b) Illustration of preferential microparticle confinement (from free-flowing nanoscale reagents) and on-particle synthesis within an actuated LSBAW microreactor.

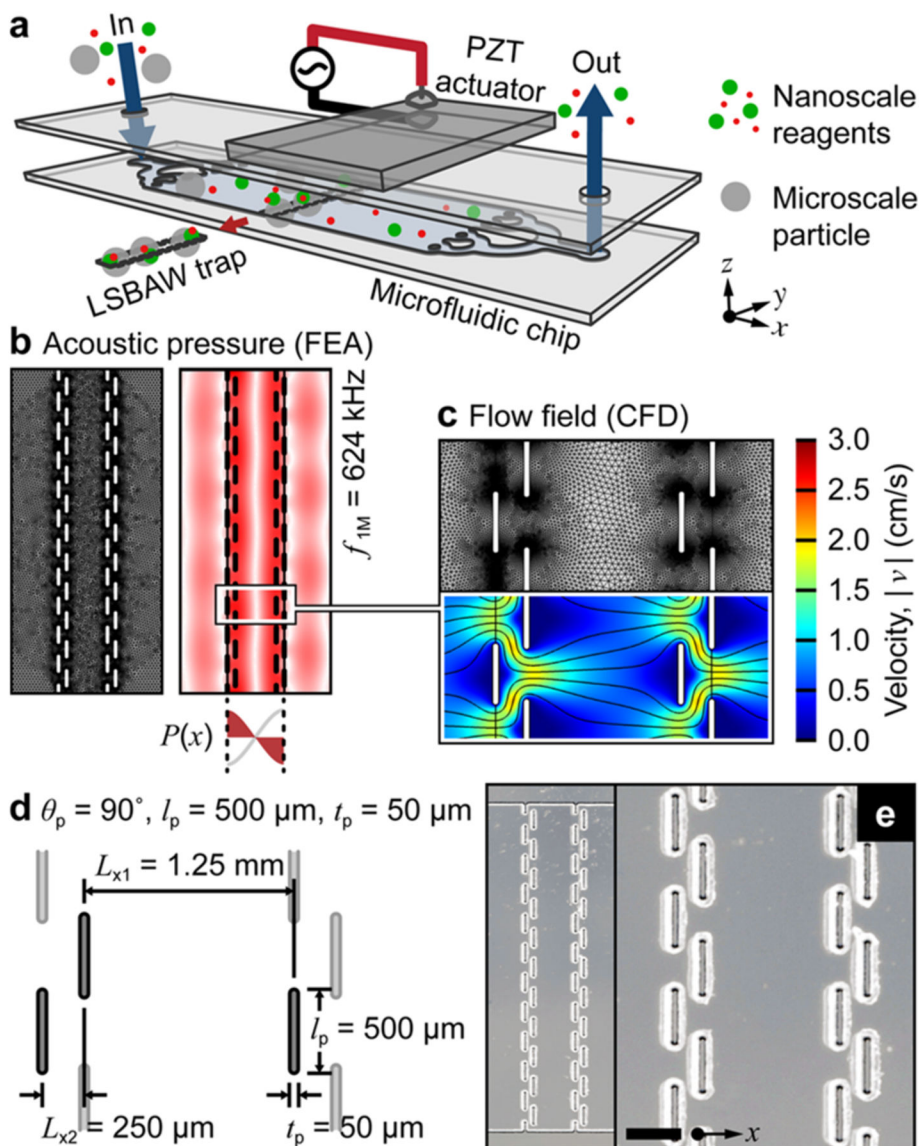


Figure 2. LSBAW microreactor design, modeling, and realization. (a) Schematic representation of the acoustic microfluidic device assembly for separation and confinement of microparticle substrates from free-flowing nanoscale reagents. (b) Model-predicted eigenshape (pressure field) at the first half-wavelength resonance of the LSBAW pillar array ($f_{1,M} = 624$ kHz). (c) Model-predicted flow field at an inflow rate of $100 \mu\text{L}/\text{min}$ (overall channel width and depth were 10.0 mm and $60 \mu\text{m}$, respectively). (d) Schematic and (e) microscope images of a glass LSBAW pillar array. Scale bar is $500 \mu\text{m}$.

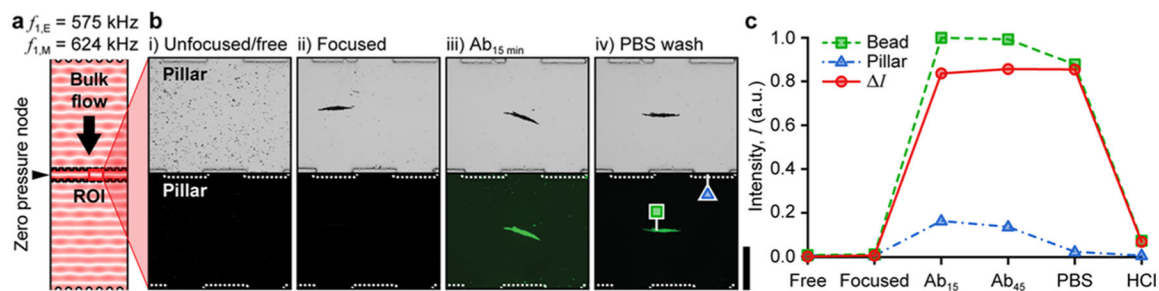


Figure 3.

On-chip antibody (Ab) capture, purification, and release using Protein G-terminated hollow glass spheres (HGSs). (a) Model-predicted acoustic pressure field at the experimentally identified operating frequency $f_{1,E} = 575$ kHz. (b) Brightfield and fluorescence micrographs of the experimental progression: (i) a uniform distribution of HGS after introduction; (ii) focused HGS at the LSBAW microreactor midline under ultrasonic actuation ($f_{1,E} = 575$ kHz, $V_E = 91$ V_{pp}); (iii) Ab-decorated HGS (Ab-HGS) after 15 min of incubation in fluorescent Ab solution (1 μ g/mL in PBS, rabbit anti-goat IgG Alexa Fluor 488); and (iv) Ab-HGS after PBS wash to remove free Ab. Scale bar is 0.5 mm. (c) Relative intensity (normalized to the highest value) of bead cluster [green square in panel b(iv), I_{bead}], pillar [blue triangle in b(iv), I_{pillar}], and intensity difference ($I = I_{\text{bead}} - I_{\text{pillar}}$) taken at five points during the experimental progression. Brightfield exposure is 1 ms, and green-channel exposure is 3 s.

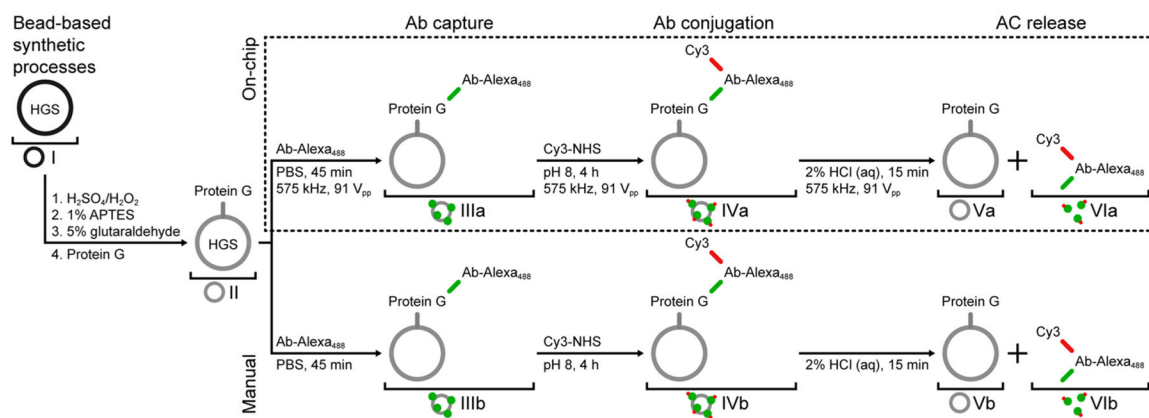


Figure 4. Process flows for LSBAW microreactor-based (on-chip) and manual antibody (Ab) conjugation. Hollow glass spheres (HGSs) are functionalized for Protein G termination prior to the synthesis. Both processes involve fluorescent Ab coupling to Protein G-terminated HGSs, labeling of Ab with Cy3 dye, and release of modified antibodies from reaction substrates; however, all on-chip processes are done under acoustic actuation and HGS confinement.

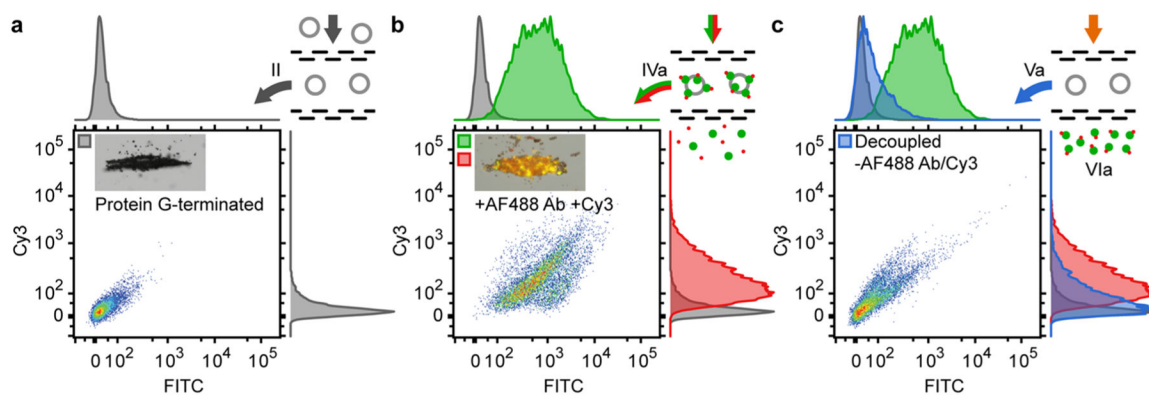


Figure 5.

Cy3 modification of AF488-labeled secondary antibodies (rabbit anti-goat IgG Alexa Fluor 488). (a) Flow cytometry intensity scatter plots and histograms (green/FITC and red/Cy3) for Protein G-terminated HGSs with brightfield image (inset) of focused microspheres ($t_{\text{exp}} = 0.25$ s). (b) Intensity scatter plots and histograms for Cy3-modified antibody-terminated HGSs (Ab-HGSs) with a composite image of brightfield ($t_{\text{exp}} = 0.25$ s), green and red channels ($t_{\text{exp}} = 2$ s). (c) Intensity scatter plots and histograms for postrelease HGSs. All scatter plots were normalized to ensure peak intensity was $<10^5$; histograms were normalized to achieve uniform peak heights.

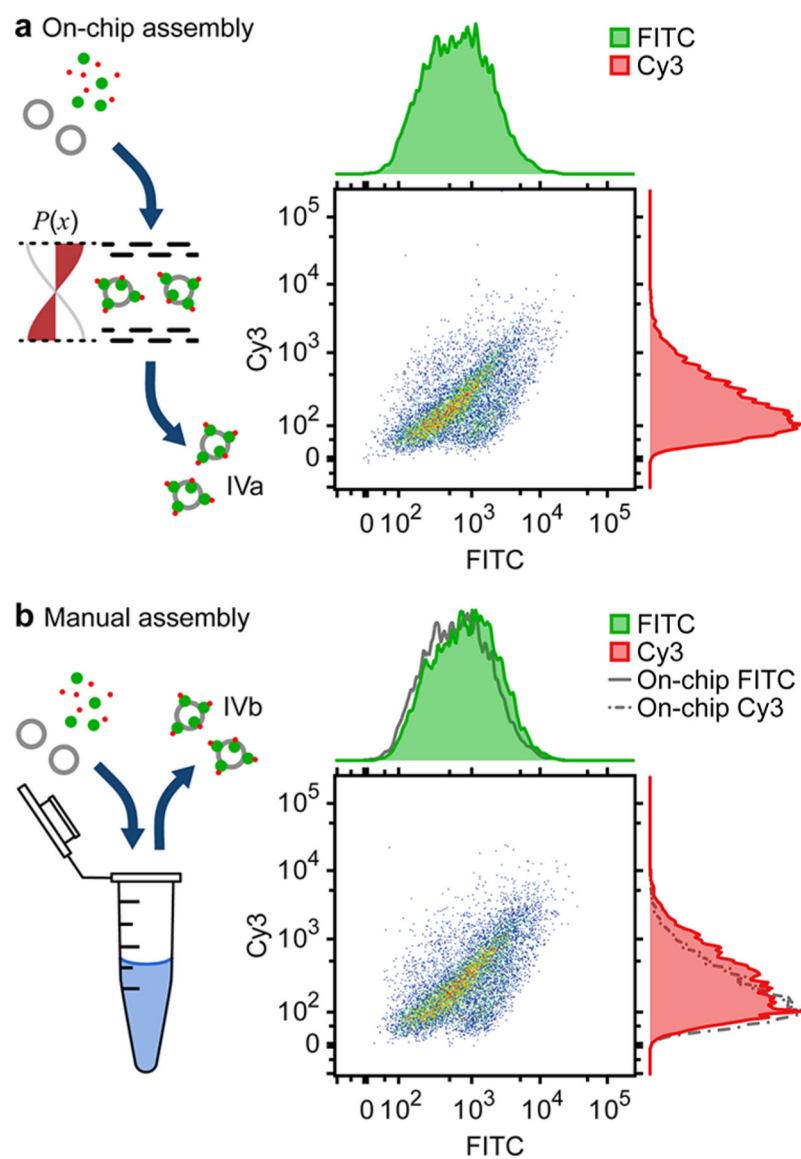


Figure 6. Validation of on-chip versus manual synthesis (Cy3 conjugation to immobilized AF488-labeled antibodies). (a) Ungated intensity scatter plots and histograms (green/FITC and red/Cy3) for LSBAW-synthesized Cy3-modified Ab-HGSs (sample **IVa**). (b) Intensity scatter plots and histograms for manually synthesized modified HGSs (sample **IVb**). Histograms corresponding to the LSBAW-based synthesis are reproduced as gray solid and dashed-dotted lines for reference. Histograms were normalized to ensure uniform height.